PAPER

Tilted Axis Rotation of ^{57}Mn in Covariant Density Functional Theory

To cite this article: Jing Peng and Wen-Qiang Xu 2016 *Chinese Phys. Lett.* **33** 012101

CHIN. PHYS. LETT. Vol. 33, No. 1 (2016) 012101

Tilted Axis Rotation of ^{57}Mn in Covariant Density Functional Theory *

Jing Peng(彭婧)[1,2**], Wen-Qiang Xu(徐文强)[1]

[1]*Department of Physics, Beijing Normal University, Beijing 100875*
[2]*State Key Laboratory of Theoretical Physics, Institute of Theoretical Physics, Chinese Academy of Sciences, Beijing 100190*

(Received 24 September 2015)

The self-consistent tilted axis cranking covariant density functional theory based on the point-coupling interaction is applied to investigate the tilted axis rotation in ^{57}Mn. The observed data for band C are reproduced well with the assigned configuration config 1. The shears mechanism for magnetic rotation is examined by investigating microscopically the orientation of angular momentum and the corresponding contributions. It is found that config 1 and config 3 correspond to a rotation of high-K character. Config 2 corresponds to a rotation of magnetic character. However, due to the presence of electromagnetic transition $B(M1)$ and $B(E2)$, collective rotation plays an essential role in the competition with magnetic rotation.

PACS: 21.60.Jz, 21.10.Re, 23.20.−g, 27.40.+z DOI: 10.1088/0256-307X/33/1/012101

Rotational phenomena exist commonly in nature. We can find many examples including the macroscopic star and the microscopic molecules. In nuclear physics, the rotation features of the nucleus were firstly noted by Teller *et al.* in 1938.[1] Subsequently, a more complete explanation of the nuclear rotation was given by Bohr *et al.*[2]

It is well known that the high angular momenta of atomic nuclei are connected with the collective rotations with a stable nuclear deformation. Such a kind of rotation is characterized by strong electric quadrupole ($E2$) transitions, in which the angular momentum is generated through small contributions from many nucleons. The study along this line has attracted general interest in nuclear physics, as evidenced by the exciting discoveries such as backbending,[3] alignment phenomena,[4,5] and superdeformed rotational bands.[6]

In the early 1990s, a new type of rotation, consisting of magnetic dipole (M1) transitions in nearly spherical nuclei, was observed in the Pb isotopes.[7–9] The name 'magnetic rotation' was introduced to account for this phenomenon and to distinguish it from the usual collective rotation in well-deformed nuclei (called electric rotation).[10] In the magnetic rotation, the energy and the angular momentum increases via the so-called 'shears mechanism',[11] i.e., by the alignments of the high-j proton and neutron angular momenta. Consequently, rotational bands can be formed despite a nucleus being nearly spherical.

Since the pioneering work on the magnetic rotation in nuclear physics, several efforts have been made to understanding this new phenomenon and to exploring the manifestation thereof in the nuclear chart. Up to now, more than 200 magnetic rotational bands spread in the mass regions of $A \sim 60$, $A \sim 80$, $A \sim 110$, $A \sim 140$, and $A \sim 190$ have already identified.[12–15]

For magnetic rotations, the axis of the uniform rotation does not coincide with any of the principal axis of the density distribution. Therefore, a description of this excitation mode requires a model beyond principal axis cranking, i.e., the tilted axis cranking (TAC) model. Even today, the TAC models[10–12] are still the main tools for studying the magnetic rotation. Moreover, the classical particle plus rotor model[13] and the shell model[16] are applied to the investigation of magnetic rotation as well. Due to the high numerical complexity of the TAC model, most of the applications are implemented on a hybrid Woods–Saxon or Nilsson model combined with the shell corrections. Until 2000, in the framework of covariant density functional theory (CDFT), a TAC code has been developed in Ref. [17]. However, due to the numerical complexity, it has only been applied for the magnetic rotation in ^{84}Rb a relatively light nucleus. Later, focusing on magnetic rotation, a two-dimensional cranking version of CDFT based on the nonlinear meson-exchange interaction was established in Ref. [18]. It has been applied to the magnetic rotation in medium heavy nucleus ^{142}Gd. Very recently, the TAC model based on a relativistic point-coupling Lagrangian has been established and applied successfully to investigate the magnetic rotation.[19–24] Note that the tilted axis cranking CDFT is not only limited to investigate the magnetic rotation, and it has been applied equally well to antimagnetic rotations,[25–30] high-K bands,[31] rotations with exotic rod shape.[32]

Despite recent experimental efforts, the high-spin data for magnetic rotation in the $A \sim 60$ mass region are still sparse. So far, the magnetic rotation has only been suggested in ^{60}Ni[19,33] and ^{60}Fe.[22] Using two separate heavy-ion fusion–evaporation reactions at Argonne National Laboratory,[34] the newly observed high spin states in nucleus ^{57}Mn provide such an example to investigate the magnetic rotation in Mn isotopes. Note that with the previous suggestion,[22]

*Supported by the National Natural Science Foundation of China under Grant No 11461141002, and the Open Project Program of State Key Laboratory of Theoretical Physics of Institute of Theoretical Physics of Chinese Academy of Sciences under Grant No Y4KF041CJ1.

**Corresponding author. Email: jpeng@bnu.edu.cn

we are focusing on the $\Delta I = 2$ high spin bands observed at $I \sim \frac{13}{2}\hbar$–$\frac{21}{2}\hbar$ above 4 MeV excitation energy in ^{57}Mn, which is labeled as band C following the notation of Ref. [34].

In this Letter, we investigate the tilted axis rotation of ^{57}Mn using the tilted axis cranking covariant density functional theory (TAC-CDFT). With the suggestion in the previous work,[34] different couplings of $f_{7/2}$ proton hole and $g_{9/2}$ neutron form three configurations $\pi f_{7/2}^{-3} \otimes \nu[g_{9/2}^{1}(fp)^3]$, $\pi[f_{7/2}^{-1}s_{1/2}^{-2}] \otimes \nu[g_{9/2}^{1}(fp)^3]$ and $\pi f_{7/2}^{-3} \otimes \nu[g_{9/2}^{2}(fp)^2]$. Based on these three configurations, the level schemes, the relation between the rotational frequency and the angular momentum are calculated and compared with the available data. The shears mechanism as well as the electromagnetic transition strengths $B(E2)$ and $B(M1)$ will also be presented.

In the TAC-CDFT, nuclei are characterized by the relativistic fields $S(\boldsymbol{r})$ and $V^{\mu}(\boldsymbol{r})$ in the Dirac equation in the rotating frame as

$$[\boldsymbol{\alpha}\cdot(-i\nabla - \boldsymbol{V}) + \beta(m+S) + V - \boldsymbol{\Omega}\cdot\hat{\boldsymbol{J}}]\psi_i = \varepsilon_i\psi_i, \quad (1)$$

where $\hat{\boldsymbol{J}} = \hat{\boldsymbol{L}} + \frac{1}{2}\hat{\boldsymbol{\Sigma}}$ is the total angular momentum of the nucleon spinors, and $S(\boldsymbol{r})$ and $V^{\mu}(\boldsymbol{r})$ are the relativistic scalar and vector fields, respectively, which are in turn coupled with the densities and currents. For more details, one can see Refs. [18,26]. We employ a spherical harmonic oscillator basis with 10 major shells to solve the Dirac equation. The point-coupling interaction PC-PK1[35] is used for the Lagrangian, and the pairing correlations are ignored. The self-consistent rotational angle is determined by requiring that $\boldsymbol{\Omega}$ is parallel with $\boldsymbol{J}$ at fixed Ω.

In this work, following the same procedures outlined in Ref. [18] we investigate the tilted axis rotation of ^{57}Mn using the TAC-CDFT, and especially focus on the possible existence of magnetic rotation in the newly observed high spin states.[34] The magnetic rotation is expected to be realized in the nucleus with few high-j orbitals of protons and neutrons. For the nucleus ^{57}Mn, the proton holes in $f_{7/2}$ orbital and the neutron particles in $g_{9/2}$ orbital could form the matched high-j configurations and the angular momentum arrangements for magnetic rotation. Since the parity of band C in ^{57}Mn cannot be determined by using the previous experimental data,[34] we adopt three configurations coming from different combinations of $\pi f_{7/2}$ and $\nu g_{9/2}$ orbitals for ^{57}Mn in the present TAC-CDFT calculation. For simplicity, the notations of config 1, config 2 and config 3 will be used to denote these three configurations hereafter. Note that the assigned configurations config 1, config 2 and config 3 here have positive, positive and negative parities, respectively. All the configurations as well as their corresponding deformation parameters are listed in Table 1 in comparison with those of the ground state for ^{57}Mn. The β and γ values for config 1, config 2 and config 3 shown here are only the values at $\hbar\Omega = 0.3$ MeV. One could see that the β deformations are not so small for all the configurations, and this indicates that the collective rotation would not be negligible. Moreover, the configuration for the ground state here has negative parity and it is consistent with the previous investigation.[34]

Table 1. Valence nucleon and unpaired nucleon configurations as well as the corresponding deformation parameters β and γ in ^{57}Mn.

Notation	Valence nucleon configuration	Unpaired nucleon configuration	β	γ
g.s.	$\pi f_{7/2}^{-3} \otimes \nu(fp)^4$	$\pi f_{7/2}^{-1}$	0.25	11.8°
Config 1	$\pi f_{7/2}^{-3} \otimes \nu[g_{9/2}^{1}(fp)^3]$	$\pi f_{7/2}^{-1} \otimes \nu[g_{9/2}^{1}(fp)^3]$	0.29	10.1°
Config 2	$\pi[f_{7/2}^{-1}s_{1/2}^{-2}] \otimes \nu[g_{9/2}^{1}(fp)^3]$	$\pi f_{7/2}^{-1} \otimes \nu[g_{9/2}^{1}(fp)^3]$	0.37	39.6°
Config 3	$\pi f_{7/2}^{-3} \otimes \nu[g_{9/2}^{2}(fp)^2]$	$\pi f_{7/2}^{-1} \otimes \nu[g_{9/2}^{2}(fp)^2]$	0.36	0.2°

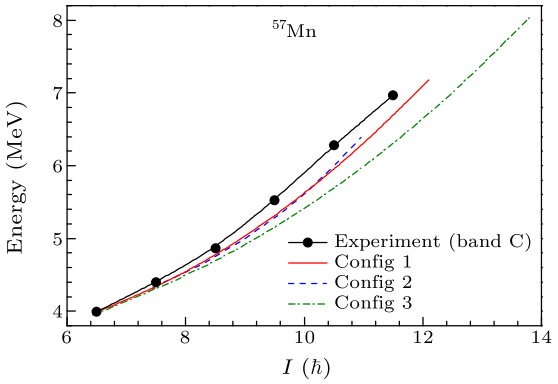

Fig. 1. (Color online) The energy spectra obtained from the TAC-CDFT calculations with config 1, config 2 and config 3 in comparison with the available data of ^{57}Mn.[34] The energies at $I = 6.5\hbar$ are taken as reference for ^{57}Mn.

In Fig. 1, the calculated energy spectra are compared with the available data[34] for ^{57}Mn. The energy at $I = 6.5\hbar$ is taken as reference for ^{57}Mn. In Fig. 1, one could clearly see that the TAC-CDFT results of config 1 and config 2 could reproduce the excitation energies for band C of ^{57}Mn. However, the assigned configuration could not be followed in the calculation up to the largest observed spin, i.e., the convergent results of config 2 could be obtained only up to around $11\hbar$. The energy displacement between config 3 and data increases with the spin.

In Fig. 2, the angular momenta I determined by the cranking condition $J = \sqrt{I(I+1)}$ are shown as a function of the rotational frequency in comparison with the data[34] of ^{57}Mn. The experimental rotational frequency can be extracted as in Ref. [36],

$$\hbar\Omega_{\rm exp} = \frac{1}{2}[E_{\gamma}(I+1 \to I) + E_{\gamma}(I \to I-1)]. \quad (2)$$

In general, all the calculated angular momenta $I(\Omega)$

form nearly straight lines. For band C in ^{57}Mn, the TAC-CDFT results of config 1 are in good agreement with the data. Note that in Fig. 2, there is a slight discrepancy at $\hbar\Omega = 0.7$ MeV between the data of band C and the result of config 1, which corresponds to the experimental upbending. Moreover, dynamic moments of inertia $\mathcal{J}^{(2)}$ $(dI/d\Omega)$ of config 2 and config 3, which is the slope of the curve $I(\Omega)$, are different from the data of band C. The slope of the curve $I(\Omega)$ of config 3 is greater than that of config 1. In contrast, the results for config 2 are of the smallest slope.

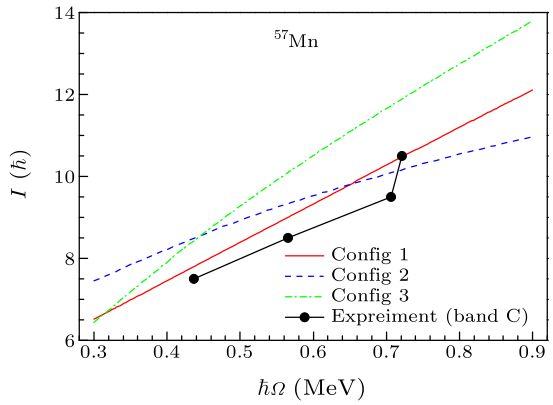

Fig. 2. (Color online) The total angular momenta as a function of the rotational frequency in the TAC-CDFT calculations with config 1, config 2 and config 3 in comparison with the data for ^{57}Mn.[34]

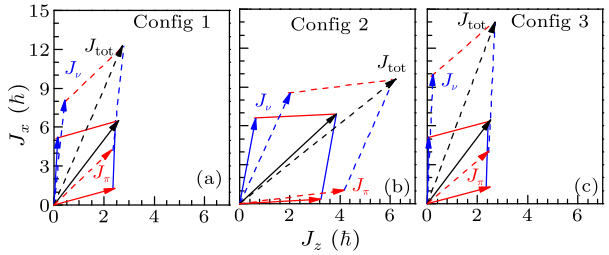

Fig. 3. (Color online) The composition of the total angular momentum at both the minimum (at $\hbar\Omega = 0.3$ MeV, solid line) and the maximum rotational frequency (at $\hbar\Omega = 0.9$ MeV, dashed line) for config 1, config 2 and config 3 in ^{57}Mn.

To examine the shears mechanism for ^{57}Mn, we show in Fig. 3 the proton and neutron angular momentum vectors ($\boldsymbol{J}_\pi$ and $\boldsymbol{J}_\nu$), as well as the total angular momentum vector $\boldsymbol{J}_{\rm tot} = \boldsymbol{J}_\pi + \boldsymbol{J}_\nu$ for config 1, config 2 and config 3. All the symbols have the same definition as in Ref. [18]. In general, for the bands built on these three configurations, the contributions to the angular momenta come mainly from the high-j orbitals, i.e., the $g_{9/2}$ neutrons and the $f_{7/2}$ protons. At the bandhead, the neutron particle(s) filling the bottom of the $g_{9/2}$ shell mainly contribute to the neutron angular momentum along the z-axis, and the proton hole at the top of the $f_{7/2}$ shell mainly contributes to the proton angular momentum along the x-axis. For config 2, the neutron and proton angular momenta form the two blades of the shears. As the frequency increases, the two blades move toward each other to provide partially larger angular momentum, while the direction of the total angular momentum stays nearly unchanged. This corresponds to the shears mechanism of magnetic rotation. For config 1 and config 3, with increasing the frequency, only proton angular momenta move obviously toward the direction of the total angular momentum while the neutron angular momenta barely change. This behavior is in accordance with the rotating bands of the high-K character, which is similar to the 'stapler bands' in Ref. [37]. On the other hand, it should be noted that the substantial increase of the neutron and proton angular momenta of config 1, config 2 and config 3 also contributes notably to the generation of the total angular momentum along the bands, which originates from the alignment generated by the collective rotation.

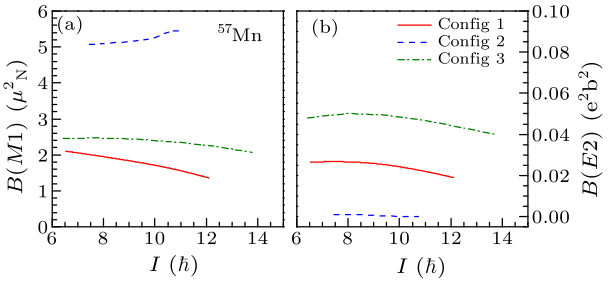

Fig. 4. (Color online) The reduced transition probabilities $B(E2)$ and $B(M1)$ as a function of the total angular momentum in the TAC-CDFT calculations with config 1, config 2 and config 3 for ^{57}Mn.

The typical characteristics of the magnetic rotation are the strongly enhanced $M1$ transitions at low angular momenta and their falling tendencies with the angular momentum. In contrast, the $E2$ transitions of the band are very weak. Here the $B(M1)$ values are derived from the relativistic form of the effective current operator.[18] In Fig. 4, the reduced transition probabilities $B(E2)$ and $B(M1)$ from the TAC-CDFT calculations with config 1, config 2 and config 3 are shown as a function of the total angular momentum. In contrast to the large $B(M1)$ values (about several μ_N^2), the $B(E2)$ values are very small for all the three bands ($< 0.05e^2b^2$). For config 1 and config 3, the smooth-decreasing tendencies of the $B(M1)$ values are obtained. For config 2, however, the $B(M1)$ values exhibit increasing tendency along the band, indicating that the collective rotation is dominant in the competition with magnetic rotation. As we know, the shears mechanism shown in Fig. 3 results in the falling tendency of $B(M1)$. On the other hand, the increase of the magnetic moment generated by collective rotation leads to the increase of $B(M1)$. Furthermore, the pairing correlations are ignored in the present calculation. As discussed in Ref. [19] the pairing correlations strongly affect the levels in the neighborhood of the Fermi surface. This causes a stronger reduction for $B(M1)$ with major contributions from the valence particles or holes. There is no experimental $B(E2)$ and $B(M1)$ values for the high-spin states in

^{57}Mn available at present, and further measurement is welcome to validate the predicted electromagnetic transition.

In summary, the self-consistent TAC-CDFT based on the point-coupling interaction has been applied to investigate the tilted axis rotation of ^{57}Mn. Based on config 1, config 2 and config 3, the energy spectra, the relation between the angular momentum and the rotational frequency, reduced $E2$ and $M1$ transition probabilities have been studied. The energy spectra and $I\Omega$ relation of band C have been well reproduced by the TAC-CDFT calculation with config 1. The shears mechanism for config 2 and the stapler mechanisms for config 1 and config 3 have been demonstrated by the orientation of neutron and proton angular momenta. The strongly enhanced $M1$ transitions and weak $E2$ transitions for config 1, config 2 and config 3 are consistent with the behavior of the neutron and proton angular momenta. Config 1 and config 3 correspond to a rotation of high-K character and the collective rotation provides a remarkable contribution to the total angular momentum as well. Config 2 corresponds to a rotation of magnetic character, while collective rotation plays an essential role in the competition with magnetic rotation.

References

[1] Teller E and Wheeler J A 1938 *Phys. Rev.* **53** 778
[2] Bohr A and Mottelson B R 1975 *Nuclear Structure* (New York: Benjamin) vol Ⅱ
[3] Johnson A, Ryde H and Sztarkier J 1971 *Phys. Lett.* B **34** 605
[4] Stephens F S and Simon R S 1972 *Nucl. Phys.* A **183** 257
[5] Banerjee B, Mang H J and Ring P 1973 *Nucl. Phys.* A **215** 366
[6] Twin P J, Nyakó B M, Nelson A H, Simpson J, Bentley M A, Cranmer-Gordon H W, Forsyth P D, Howe D, Mokhtar A R, Morrison J D, Sharpey-Schafer J F and Sletten G 1986 *Phys. Rev. Lett.* **57** 811
[7] Clark R M, Wadsworth R, Paul E S, Beausang C W, Ali I, Astier A, Cullen D M, Dagnall P J, Fallon P, Joyce M J, Meyer M, Redon N, Regan P H, Nazarewicz W and Wyss R 1992 *Phys. Lett.* B **275** 247
[8] Baldsiefen G, Hübel H, Mehta D, Thirumala Rao B V, Birkental U, Fröhlingsdorf G, Neffgen M, Nenoff N, Pancholi S C, Singh N, Schmitz W, Theine K, Willsau P, Grawe H, Heese J, Kluge H, Maier K H, Schramm M, Schubart R and Maier H J 1992 *Phys. Lett.* B **275** 252
[9] Kuhnert A, Stoyer M A, Becker J A, Henry E A, Brinkman M J, Yates S W, Wang T F, Cizewski J A, Stephens F S, Deleplanque M A, Diamond R M, Macchiavelli A O, Draper J E, Azaiez F, Kelly W H and Korten W 1992 *Phys. Rev.* C **46** 133
[10] Frauendorf S, Meng J and Reif J 1994 *Proc. Conf. Phys. From Large $\gamma-$ray Detector Arrays* (Berkeley LBL-35687, August 1994) Ⅱ p 52
[11] Frauendorf S 1993 *Nucl. Phys.* A **557** 259
[12] Frauendorf S 2001 *Rev. Mod. Phys.* **73** 463
[13] Clark R M and Macchiavelli A O 2000 *Annu. Rev. Nucl. Part. Sci.* **50** 1
[14] Hübel H 2005 *Prog. Part. Nucl. Phys.* **54** 1
[15] Meng J, Peng J, Zhang S Q and Zhao P W 2013 *Front. Phys.* **8** 55
[16] Frauendorf S, Reif J and Winter G 1996 *Nucl. Phys.* A **601** 41
[17] Madokoro H, Meng J, Matsuzaki M and Yamaji S 2000 *Phys. Rev.* C **62** 061301
[18] Peng J, Meng J, Ring P and Zhang S Q 2008 *Phys. Rev.* C **78** 024313
[19] Zhao P W, Zhang S Q, Peng J, Liang H Z, Ring P and Meng J 2011 *Phys. Lett.* B **699** 181
[20] Li C B, Li J, Wu X G, Li X F, Zheng Y, He C Y, Li G S, Yao S H, Yu B B, Cao X P, Hu S P, Wang J L, Xu C and Cheng Y Y 2012 *Nucl. Phys.* A **892** 34
[21] Yu L F, Zhao P W, Zhang S Q, Ring P and Meng J 2012 *Phys. Rev.* C **85** 024318
[22] Steppenbeck D, Janssens R V F, Freeman S J, Carpenter M P, Chowdhury P, Deacon A N, Honma M, Jin H, Lauritsen T, Lister C J, Meng J, Peng J, Seweryniak D, Smith J F, Sun Y, Tabor S L, Varley B J, Yang Y C, Zhang S Q, Zhao P W and Zhu S 2012 *Phys. Rev.* C **85** 044316
[23] Peng J and Xing L F 2009 *Chin. Phys. Lett.* **26** 032101
[24] Peng J, Yao J M, Zhang S Q and Meng J 2010 *Chin. Phys. Lett.* **27** 122101
[25] Zhao P W, Peng J, Liang H Z, Ring P and Meng J 2011 *Phys. Rev. Lett.* **107** 122501
[26] Zhao P W, Peng J, Liang H Z, Ring P and Meng J 2012 *Phys. Rev.* C **85** 054310
[27] Li X W, Li J, Lu J B, Ma K Y, Wu Y H, Zhu L H, He C Y, Li X Q, Zheng Y, Li G S, Wu X G, Ma Y J and Liu Y Z 2012 *Phys. Rev.* C **86** 057305
[28] Zhang P, Qi B and Wang S Y 2014 *Phys. Rev.* C **89** 047302
[29] Peng J and Zhao P W 2015 *Phys. Rev.* C **91** 044329
[30] Peng J, Zhao P W, Zhang S Q and Meng J 2015 arXiv:1508.06987v1[nucl-th]
[31] Zhao P W, Zhang S Q and Meng J 2015 *Phys. Rev.* C **92** 034319
[32] Zhao P W, Itagaki N and Meng J 2015 *Phys. Rev. Lett.* **115** 022501
[33] Torres D A, Cristancho F, Andersson L L, Johansson E K, Rudolph D, Fahlander C, Ekman J, Rietz R du, Andreoiu C, Carpenter M P, Seweryniak D, Zhu S, Charity R J, Chiara C J, Hoel C, Pechenaya O L, Reviol W, Sarantites D G, Sobotka L G, Baktash C, Yu C H, Carlsson B G and Ragnarsson I 2008 *Phys. Rev.* C **78** 054318
[34] Steppenbeck D, Deacon A N, Freeman S J, Janssens R V F, Zhu S, Carpenter M P, Chowdhury P, Honma M, Lauritsen T, Lister C J, Seweryniak D, Smith J F, Tabor S L and Varley B J 2010 *Phys. Rev.* C **81** 014305
[35] Zhao P W, Li Z P, Yao J M and Meng J 2010 *Phys. Rev.* C **82** 054319
[36] Frauendorf S and Meng J 1996 *Z. Phys.* A **356** 263
[37] Chen Z Q, Wang S Y, Liu L, Zhang P, Jia H, Qi B, Wang S, Sun D P, Liu C, Li Z Q, Wu X G, Li G S, He C Y, Zheng Y and Zhu L H 2015 *Phys. Rev.* C **91** 044303